J Electr Eng Technol.2015;10(1): 314-319
http://dx.doi.org/10.5370/JEET.2015.10.1.314

ISSN(Print) 1975-0102
ISSN(Online) 2093-7423

A Numerically Efficient Full Wave Analysis of Circular Resonators Microbandes Stacked Involving Multimetallisations

F. Chebbara† and T. Fortaki*

Abstract – The conventional geometry of a plate microstrip resonator is made up of a single metallic patch, which is printed on a monolayer dielectric substrate. Its arrangement is simple and easy to make, but it is limited in its functional abilities. Many searches have been realized to improve the bandwidth and the gain of the microstrip resonators. Among the various configurations proposed in the open literature, the stacked geometry seems to be very promising. By appropriate design, it is able to provide the operation in dual frequency mode, wide bandwidth enough and high gain. The theoretical investigations of structures composed of two stacked anti-reflection coatings, enhanced metallic coatings are available in the literature, however, for the stacked configurations involving three metallic coatings or more, not to exact or approximate analysis was conducted due to the complexity of the structure.

Keywords: Staked**,** Ground plane, Isotropy, Galerkin method, the magnetic wall cavity, Circular microstrip, Patch

1. Introduction

The microstrip antenna, originally consisting of a substrate layer with a radiating element, which is printed on a side and a ground plane on the other, is currently in evolution in the structures to dielectric multilayer substrates [1-7]. The use of multiple dielectric layers offers additional degrees of freedom to the designer who can control and optimize the performance of the antenna such as the bandwidth, the aperture of the radiation beam, the gain and others. Also, the tendencies towards plate antenna arrays indicate that microstrip antennas in the future will be largely based on multilayer technology. Given this increasing technological significance of multilayer substrates in the of plate antennas domain, to analyze these antennas the models developed should be able to hold the multilayer structures.

In the first sub-section, we study the resonance characteristics of a conventional circular microstrip resonator (single patch on a substrate monolayer). In the second sub-section, we complete the analysis in [7-9]. And on the behavior of the dual-frequency microstrip resonator formed by a stack of two circular patches, in examining the behavior of a dual-frequency microstrip resonator formed by a stack of two circular discs. In the third sub-section, we give for the first time, numerical results concerning the behavior of a dual-frequency microscript resonator formed by a stack of three circular disks. Finally, the conclusions drawn from this study are summarized in Section 5.

† Corresponding Author: Dept. of Electronic and Telecommunications, Ouargla University, Algeria. (chebbara.fo@univ-ouargla.dz)
* Dept. of Electronic and Telecommunications, Ouargla University, Algeria. (chfouad@hotmail.com)
Received: October 14, 2013; Accepted: August 21, 2014

2. Theory

The problem to solve is shown in (Fig. 1.) where we have three circular stacked microstrip patches of radii: a_1, a_2 and a_3, fabricated on a multilayer substrate (Although we show that this theory is valid for an arbitrary number of patches). The circular discs and the ground plane are assumed to be perfect conductors of a negligible thickness and the layers are of infinite extension. The multilayer medium consists of N dielectric layers having uniaxial anisotropy with the normal optical axis to the patch. Thickness of each layer: $d_j = z_j - z_{j-1}$ (j =1,2,…, N) is characterized by the vacuum permeability μ_0 and the permittivity tensor $\overline{\varepsilon}_j$ which is of the form:

$$\varepsilon_j = \varepsilon_0 \begin{pmatrix} \varepsilon_{xj} & 0 & 0 \\ 0 & \varepsilon_{xj} & 0 \\ 0 & 0 & \varepsilon_{zj} \end{pmatrix} \quad (1)$$

ε_0 is the free-space permittivity and diag stands for the diagonal matrix with the diagonal elements appearing between the brackets. Eq. (1) can be specialized to the isotropic substrate by allowing $\varepsilon_{xj} = \varepsilon_{zj} = \varepsilon_{rj}$. The circular patch is embedded in the stratification at the interface plane $z = z_p$.

All fields and currents are in harmonic regime with the $e^{i\omega t}$ dependence.

Consider $\mathbf{J}^i(\rho, \varphi) = [J_\rho^i(\rho, \varphi) J_\varphi^i(\rho, \varphi)]^T$ the areal density current on the circular disk of radius a_i. As well, $E^i(\rho, \varphi, z_{p_i}) = [E_\rho^i(\rho, \varphi, z_{p_i}) E_\varphi^i(\rho, \varphi, z_{p_i})]^T$ the value of the transverse electric field at the plane of the patch of radius a_i. In reason of the symmetric revolution of the multilayer medium around the z axis in Fig. 1, when the

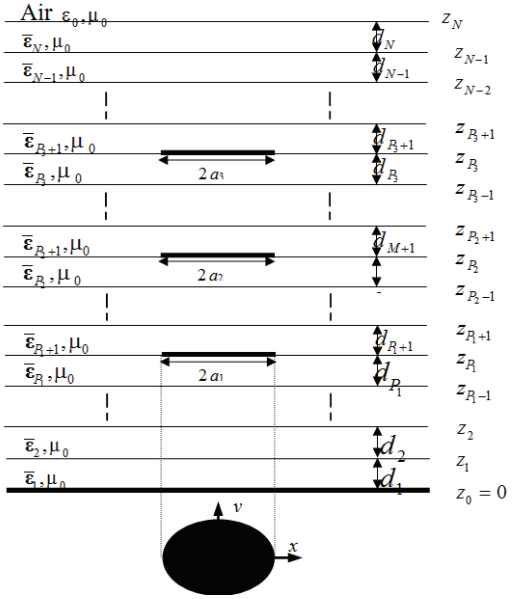

Fig. 1. Geometry of three circular discs stacked in a multilayer dielectric medium containing isotropic and / or anisotropic material

Helmholtz equations for the longitudinal components of the E_z and H_z fields are solved in cylindrical coordinates in each layer of this medium, it turns out that the E_z and H_z dependence on the φ coordinate is of $e^{ik\varphi}$ type (where k is an integer). As a result, $J^i(\rho,\varphi)$ and $E^i(\rho,\varphi,z_{p_i})$ can be written as:

$$J^i(\rho,\varphi) = \sum_{k=-\infty}^{+\infty} e^{\mathrm{i}\,k\varphi} J_k^i(\rho) \tag{2}$$

$$E^i(\rho,\beta,z_{p_i}) = \sum_{k=-\infty}^{+\infty} e^{\mathrm{i}\,k\varphi} E_k^i(\rho,z_{p_i}) \tag{3}$$

Following mathematical reasoning similar to [10-11]. We obtain a relationship, in the spectral data, between $\mathbf{J}^1(\rho,\varphi)$, $\mathbf{J}^2(\rho,\varphi)$, $\mathbf{J}^3(\rho,\varphi)$ and $E^1(\rho,\varphi,z_{p_1})$, $E^2(\rho,\varphi,z_{p2})$, $E^3(\rho,\varphi,z_{p_3})$, respectively, as:

$$\begin{aligned}\mathbf{e}_k^1(k_\rho,z_{P_1}) &= \bar{\mathbf{G}}^{11}(k_\rho)\,.\,\mathbf{j}_k^1(k_\rho)\\ &+\bar{\mathbf{G}}^{12}(k_\rho)\,.\,\mathbf{j}_k^2(k_\rho)\\ &+\bar{\mathbf{G}}^{13}(k_\rho)\,.\,\mathbf{j}_k^3(k_\rho)\end{aligned} \tag{4}$$

$$\begin{aligned}\mathbf{e}_k^2(k_\rho,z_{P_2}) &= \bar{\mathbf{G}}^{21}(k_\rho)\,.\,\mathbf{j}_k^1(k_\rho)\\ &+\bar{\mathbf{G}}^{22}(k_\rho)\,.\,\mathbf{j}_k^2(k_\rho)\\ &+\bar{\mathbf{G}}^{23}(k_\rho)\,.\,\mathbf{j}_k^3(k_\rho)\end{aligned} \tag{5}$$

$$\begin{aligned}\mathbf{e}_k^3(k_\rho,z_{P_3}) &= \bar{\mathbf{G}}^{31}(k_\rho)\,.\,\mathbf{j}_k^1(k_\rho)\\ &+\bar{\mathbf{G}}^{32}(k_\rho)\,.\,\mathbf{j}_k^2(k_\rho)\\ &+\bar{\mathbf{G}}^{33}(k_\rho)\,.\,\mathbf{j}_k^3(k_\rho)\end{aligned} \tag{6}$$

$\mathbf{j}_k^i(k_\rho)$ and $\mathbf{e}_k^i(k_\rho,z_{P_i})$ are, respectively, the Hankel transform vectors of $\mathbf{J}_k^i(\rho)$ and $\mathbf{E}_k^i(\rho,z_{p_i})$; the *nm* part of the spectral dyadic Green function is given by

$$\begin{aligned}\bar{\mathbf{G}}^{nm}(k_\rho) &= \bar{\mathbf{\Gamma}}_{<n}^{12}\cdot\left[\,\bar{\mathbf{g}}_0.\bar{\mathbf{\Gamma}}_{>m}^{12}-\bar{\mathbf{\Gamma}}_{>m}^{22}\right]\cdot\left[\,\bar{\mathbf{g}}_0\,.\,\bar{\mathbf{\Gamma}}_{=}^{12}-\bar{\mathbf{\Gamma}}_{=}^{22}\right]^{-1}\\ &= \bar{\mathbf{G}}^{mn}(k_\rho)\\ &\qquad n=1,...,3;\ m=n,...,3\end{aligned} \tag{7}$$

with

$$\bar{\mathbf{\Gamma}}_{<n} = \prod_{j=P_n}^{1}\bar{\mathbf{T}}_j\ ,\quad \bar{\mathbf{\Gamma}}_{>m} = \prod_{j=N}^{P_m+1}\bar{\mathbf{T}}_j$$

and $$\bar{\mathbf{\Gamma}}_{=} = \prod_{j=N}^{1}\bar{\mathbf{T}}_j \tag{8}$$

In Eq. (8) $\bar{\mathbf{T}}_j$ is the matrix representation of the j^{th} layer in the representation (TM, TE), is given by

$$\begin{aligned}\bar{\mathbf{T}}_j &= \begin{bmatrix}\bar{\mathbf{T}}_j^{11} & \bar{\mathbf{T}}_j^{12}\\ \bar{\mathbf{T}}_j^{21} & \bar{\mathbf{T}}_j^{22}\end{bmatrix}\\ &= \begin{bmatrix}\cos\bar{\boldsymbol{\theta}}_j & -i\,\bar{\mathbf{g}}_j^{-1}\cdot\sin\bar{\boldsymbol{\theta}}_j\\ -i\,\bar{\mathbf{g}}_j\cdot\sin\bar{\boldsymbol{\theta}}_j & \cos\bar{\boldsymbol{\theta}}_j\end{bmatrix}\\ \bar{\boldsymbol{\theta}}_j &= \bar{\mathbf{k}}_{zj}\,d_j\end{aligned} \tag{9}$$

$$\bar{\mathbf{k}}_{zj} = \mathrm{diag}\left[k_{zj}^e, k_{zj}^h\right] \tag{10}$$

$$\bar{\mathbf{g}}_j(\mathbf{k}_s) = \mathrm{diag}\left[\frac{\omega\varepsilon_0\varepsilon_{xj}}{k_{zj}^e},\ \frac{k_{zj}^h}{\omega\mu_0}\right] \tag{11}$$

In Eq. (10), k_{zj}^e and k_{zj}^h are, respectively, the propagation constants of the TE and TM waves in the j^{th} layer. They are defined by the following equations:

$$\begin{aligned}k_{zj}^e &= \sqrt{\varepsilon_{xj}k_0^2-\frac{\varepsilon_{xj}}{\varepsilon_{zj}}k_s^2}\\ k_{zj}^h &= \sqrt{\varepsilon_{xj}k_0^2-k_s^2}\quad\text{and}\quad k_0^2=\omega\sqrt{\varepsilon_0\,\mu_0}\end{aligned} \tag{12}$$

For any number of layers in the stacked configuration, the new explicit expression, shown in Eq. (7), allows easy calculation of dyadic Green functions via simple matrix multiplication. It is also important to note that the expression (7) is valid for stacked structures with more than three patches (four patches and more). Now, that we have the necessary dyadic Green functions, the Ritz-Galerkin procedure may be applied to Eqs. (4), (5) and (6) leading to a homogeneous system. This homogeneous system has nontrivial solutions when:

$$\Delta(\bar{\Omega}_n(\omega)) = 0 \tag{13}$$

where $\bar{\Omega}_n$ is the impedance matrix of the homogeneous system. Equation (13) is an equation to own ω, from which the characteristics of the stacked structure shown in Fig.1 can be obtained. In fact, if we denote:

$\omega_{nm} = 2\pi(f_r^{nm} + if_i^{nm})$ $(n = 0, \pm1, \pm2, ...; m = 1, 2, 3, ...)$ the set of complex roots of equation (13). In this case, the amounts f_r^{nm} refer to the resonant frequencies of the resonant modes of the plate circular microstrip; the amounts $BW_{nm} = 2f_i^{nm} / f_r^{nm}$ refer to the bandwidth and quantity $Q_{nm} = f_r^{nm} / 2f_i^{nm}$ designate quality factors [12]. Since $f_r^{nm} = f_r^{-n,m}$ and $f_i^{nm} = f_i^{-n,m}$, without loss of generality, in what follows, we always assume that $n \geq 0$. Note that this result is not valid in the case of ferrite-based materials; they are a part of the multilayer substrate. This behavior is attributed to the non-reciprocal ferrite and is predicted by the cavity model of a circular plate which is printed on a ferrite substrate [13, 14].

3. Approximation of Current Densities on the Circular Discs

Current densities on the three circular disks are approximated using basis functions formed by the complete orthogonal set of the TM and TE modes of a cylindrical cavity of radii a_i (a_1 for the first disc, a_2 the second disc and the third disc a_3) with lateral magnetic and electrical walls at the top and the base. These modes of currents, which, are nonzero only on the three circular disks are given by:

$$\boldsymbol{\Psi}_{np_1}(\rho) = \begin{bmatrix} J_n'(\beta_{np_1}\rho/a_1) \\ \dfrac{in a_1}{\beta_{np_1}\rho} J_n(\beta_{np_1}\rho/a_1) \end{bmatrix} \text{ and}$$

$$\boldsymbol{\Phi}_{nq_1}(\rho) = \begin{bmatrix} \dfrac{-i n a_1}{\alpha_{nq_1}\rho} J_n(\alpha_{nq_1}\rho/a_1) \\ J_n'(\alpha_{nq_1}\rho/a_1) \end{bmatrix} \quad (14)$$

$$\boldsymbol{\Psi}_{np_2}(\rho) = \begin{bmatrix} J_n'(\beta_{np_2}\rho/a_2) \\ \dfrac{in a_2}{\beta_{np_2}\rho} J_n(\beta_{np_2}\rho/a_2) \end{bmatrix} \text{ and}$$

$$\boldsymbol{\Phi}_{nq_2}(\rho) = \begin{bmatrix} \dfrac{-i n a_2}{\alpha_{nq_2}\rho} J_n(\alpha_{nq_2}\rho/a_2) \\ J_n'(\alpha_{nq_2}\rho/a_2) \end{bmatrix} \quad (15)$$

$$\boldsymbol{\Psi}_{np_3}(\rho) = \begin{bmatrix} J_n'(\beta_{np_3}\rho/a_3) \\ \dfrac{in a_3}{\beta_{np_3}\rho} J_n(\beta_{np_3}\rho/a_3) \end{bmatrix} \text{ and}$$

$$\boldsymbol{\Phi}_{nq_3}(\rho) = \begin{bmatrix} \dfrac{-i n a_3}{\alpha_{nq_3}\rho} J_n(\alpha_{nq_3}\rho/a_3) \\ J_n'(\alpha_{nq_3}\rho/a_3) \end{bmatrix} \quad (16)$$

$n = 0, +1, +2, ...$

$\boldsymbol{\Psi}_{np_1}(\rho)$ $(p_1 = 1, 2, ..., P_1)$, $\boldsymbol{\Psi}_{np_2}(\rho)$ $(p_2 = 1, 2, ..., P_2)$ and $\boldsymbol{\Psi}_{np_3}(\rho)$ $(p_3 = 1, 2, ..., P_3)$ correspond to the resonant cavity TM modes and $\boldsymbol{\Phi}_{nq_1}(\rho)$ $(q_1 = 1, 2, ..., Q_1)$, $\boldsymbol{\Phi}_{nq_2}(\rho)$ $(q_2 = 1, 2, ..., Q_2)$ and $\boldsymbol{\Phi}_{nq_3}(\rho)$ $(q_1 = 1, 2, ..., Q_3)$ correspond to the cavity resonant TE modes.

The constants: β_{np_1}, β_{np_2}, β_{np_3}, α_{nq_1}, α_{nq_2} and α_{nq_3} correspond to p_1th, p_2th, p_3th, q_1th, q_2th et q_3th zeros of $J_n'(\beta_{np_1}) = 0$, $J_n'(\beta_{np_2}) = 0$, $J_n'(\beta_{np_3}) = 0$, $J_n(\alpha_{nq_1}) = 0$, $J_n(\alpha_{nq_2}) = 0$ and $J_n(\alpha_{nq_3}) = 0$, respectively.

4. Numerical Results and Discussion

Although the Full-wave analysis presented in this part is able to give numerical results for the different modes. In what follows, we just present numerical results concerning the mode (TM11). We divide this section into three subsections. In the first sub-section, we study the resonance characteristics of the conventional circular microstrip resonator (single patch on a monolayer substrate). In the second sub-section: we complete the analysis in [7-9] and on the behavior of the dual-frequency microstrip resonator formed by a stack of two circular patches, by examining the behavior of a dual-frequency microstrip resonator formed by a stack of two circular discs. In the third sub-section, we present numerical results concerning the behavior of a dual-frequency microstrip resonator formed by a stack of three circular disks.

4.1 Conventional circular microstrip resonator

In the case of a conventional circular disk (see Fig. 2), convergent results for the resonant frequency, the bandwidth and the quality factor are obtained with $(P = 5, Q = 4)$. To validate the proposed method for the case of a circular disk printed on a single monolayer substrate, we compare in Tables 1 and 2 our numerical results with the results of Fittage curves [15]. The radius of the disc is a = 0.5 cm. In the Table 1 the substrate's material is the Duroid, while in Table 2, it is the Plexiglas. From the two tables, it is clear that our calculations of the resonance frequency and of the quality factor coincide with those of Chew [15]. The numerical results indicate that the increase of the thickness of the substrate results in a decrease of the operating frequency and the quality factor of the resonator. This means that the increase in thickness can increases the

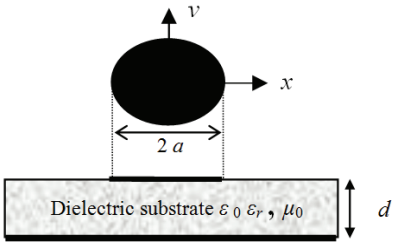

Fig. 2. Geometry of a circular microstrip printed on a monolayer dielectric substrate.

Table 1. Comparison of the resonance frequencies and quality factors calculated with the data from the literature, for a circular line resonator formed on a substrate made of Duroid; a =0.5cm, $\varepsilon_r = 2.32$.

Duroid thickness (mm)	Resonance frequencies f_r^{11} (GHz), Quality factors Q_{11}			
	W.C. Chew [15] Our results			
	f_r^{11}	Q_{11}	$f_r^{11}(GHz)$	Q_{11}
0.1	11.424	168.004	11.415	179.092
0.2	11.311	84.087	11.308	87.968
0.3	11.201	56.114	11.199	58.493
0.4	11.099	42.147	11.091	43.578
0.5	11.000	33.766	10.984	34.744
0.6	10.903	28.177	10.880	28.852
0.7	10.809	24.184	10.778	24.642
0.8	10.717	21.188	10.680	21.514
0.9	10.625	18.852	10.584	19.060
1	10.534	16.979	10.490	17.114
1.1	10.442	15.441	10.399	15.521

Table 2. Comparison of the resonance frequencies and quality factors calculated with the data from the literature, for a circular line resonator formed on a substrate made of Plexiglas; a =0.5cm, $\varepsilon_r = 2.6$.

Plexiglas thickness (mm)	Resonance frequencies f_r^{11} (GHz), Quality factors Q_{11}			
	W. C. Chew [15] Our results			
	f_r^{11}	Q_{11}	$f_r^{11}(GHz)$	Q_{11}
0.1	10.809	188.164	10.798	195.746
0.2	10.716	93.894	10.708	98.015
0.3	10.626	62.485	10.613	64.613
0.4	10.538	46.786	10.517	48.085
0.5	10.452	37.372	10.422	38.278
0.6	10.367	31.097	10.328	31.685
0.7	10.283	26.616	10.235	27.038
0.8	10.199	23.254	10.145	23.551
0.9	10.116	20.640	10.056	20.830
1	10.033	18.548	9.969	18.676
1.1	9.950	16.835	9.884	16.906

bandwidth initially very close.

4.2 Resonator formed by a stack of two circular discs

A more complex configuration, consisting of two circular discs in a stacked configuration (see Fig. 3), offers new performance that are not usually obtained by the single-disk configuration single dielectric. These performances include high gain, wide-bandwidth, dual frequency characteristics.

In order to validate the proposed theory, in the case of two stacked circular discs, numerical results were obtained for the parameters used in the Long and Walton experiment [16]. The two dielectric substrates in Fig. 3 are the same $(\varepsilon_{r1} = \varepsilon_{r2} = 2.47$ and $d_1 = d_2 = 750\ \mu m)$ and the radius of the lower disc is of a_1 =18.9mm, while that of the higher one is to be variable. In Table 3, we report both (lower f_l^{11} and greater f_u^{11}) resonances. It is observed from these

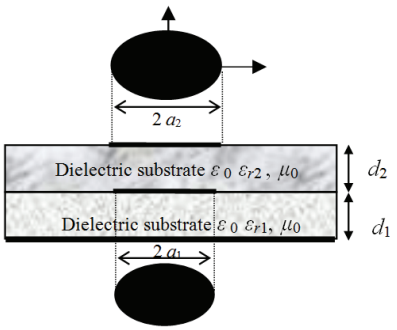

Fig. 3. Geometry of a stack composed of two circular discs made of a bilayer dielectric substrate.

Table 3. Lower and upper resonance mode TM11 of a strip line resonator formed by a stack of two circular discs microstrip

Plexiglas radius of theupper disc(mm)	Resonance frequencies f_r^{11} (GHz), Lower resonance $f_l^{11}(GHz)$ Higher resonance $f_u^{11}(GHz)$			
	Long and Walton [16]		Our results	
	f_l^{11}	f_u^{11}	f_l^{11}	f_u^{11}
17.5	2.853	3.338	2.854	3.341
18.75	2.830	3.120	2.829	3.117
18.9	2.825	3.110	2.818	3.107
19.25	2.804	3.060	2.805	3.069
20	2.728	3.009	2.731	3.006

comparisons that the agreement between theory and experiment is excellent.

Finally, it is important to note that from the different executions of the developed program, we conclude that the two resonators constituting the stacked structure, which determine the behavior of the dual frequency resonator depends on the relative sizes of the circular discs. In the case, where the radius of the upper disk is larger than that of the lower disc, less resonance is associated with the resonator formed by the upper disc and the ground plane, and the upper resonance is connected to the lower disk. The lower resonance is very close to the resonance frequency of the upper disk isolated. In the case, where the radius of the upper disk is smaller than that of the lower disc, the lower resonance is associated with the resonator formed by the lower disc and the ground plane and the upper resonance is associated with the resonator formed by the two discs circular. Now, the lower resonance is very close to the resonance frequency of the lower disk isolated (i.e. the lower disc substrate in the configuration substrate-substrate). These behaviors are in agreement with those found theoretically for the case of a structure stacked microstrip formed of two circular patches [7-9].

4.3 Resonator formed by a stack of three circular discs

In this sub-section, we apply the formulation of the Section II to study the resonance characteristics of the

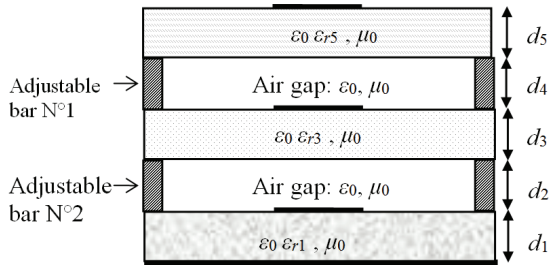

Fig. 4. Geometry of the stacked microstrip configuration used in the experiment of Revankar and Kumar [17]

stacked geometry shown in Fig. 4.

In order to have the characteristic of an adjustable resonance, two adjustable air gaps are inserted into the configuration. The first air gap is located just on the first circular disc, while the second air gap is located on the second circular disc. The first disk (of radius a_1) is printed on a substrate (of thickness d_1 and relative permittivity ε_{r1}).

The second disc (of radius a_2) is printed on a substrate (of thickness d_3 and relative permittivity ε_{r3}). The third disc (of radius a_3) is printed on a substrate (of thickness d_5 and relative permittivity ε_{r5}).

Numerical results are obtained for the parameters used in the Revankar and Kumar experiment [17], for $a_1 = a_2 = a_3 =$ 1.65cm, $\varepsilon_{r1} = 2.33$, $\varepsilon_{r3} = 2.45$, $\varepsilon_{r5} = 2.2$, d_1 =1.58mm, d_2 = 4mm, d_3 = 0.762mm and d_4 = 0.508mm.

The antenna is therefore characterized by the variation of the air separation d_4. With respect to Microstrip resonators having single disk, the phenomenon of spurious resonances is much more noticeable in microstrip resonators with stacking configurations. The calculated resonance frequencies of the TM_{11} mode are shown in Table 4 and are compared with measured values of Revankar and Kumar [17]. The presence of parasitic disks introduces two resonances: lower and higher resonances. Note that the measured resonance frequencies f_l^{11} and f_u^{11} given in Table 4 are obtained from the curves "Return loss". It is observed that the difference between our calculated resonance frequencies and the measured data is estimated by 6.06% at most. Therefore, a good agreement between theory and experiment is achieved.

Finally, it is important to note that the presence of three circular discs in a stacked configuration of Fig. 4 indicates the presence of three resonant cavities. This led us to automatically think that the stacked structure in Fig. 4 has three resonances. Although the numerical results in Table 4 indicate the presence of only two resonances, we think that it is important to examine, more carefully, the resonance of a microstrip structure formed by a stack of three metal patches.

Table 4. Lower and upper resonance mode TM11 of a strip line resonator formed by a stack of two circular discs microstrip

Air separation (μm)	Resonance frequencies (GHZ)			
	Revankar and Kumar [17]		Our results	
	f_l^{11}	f_u^{11}	f_l^{11}	f_u^{11}
1000	3.300	3.775	3.251	3.824
2000	3.272	3.700	3.228	3.761
5200	3.312	3.457	3.264	3.391
6400	3.282	3.425	3.239	3.486

5. Conclusion

In this paper, we have presented a numerical model of a microstrip resonator formed by a stack of arbitrary number of patches. It combines both precision and computing speed and allows the calculation of: resonant frequencies, bandwidths and quality factors. The circular discs are produced in a medium containing isotropic and / or anisotropic multilayer nonmagnetic materials. The contributions in this paper can be summarized as follows:

- The new explicit formulas have been developed for the calculation of spectral dyadic Green's functions of microstrip resonator formed by a stack of an arbitrary number of the circular discs. These circular discs are embedded in a multilayered dielectric medium containing isotropic and / or anisotropic materials.
- By transforming the system of Cartesian axes towards the (TM, TE) representation, the new formulas of dyadic Green spectral functions are valid for both circular geometries for rectangular geometries.
- The origin of the behavior of a dual-frequency microstrip resonator formed by a stack of two circular microstrip disks has been explained in detail. Indeed, the resonant cavities responsible for lower and upper resonances were clearly marked.
- Numerical results related to the behavior of a dual-frequency microstrip resonator formed by a stack of three circular discs were given and argued.

In the triple Frequency operation mode, where the antenna operates efficiently in three distinct frequencies, is sometimes of an extreme need in some civil or military applications. For the research of structures to this type of operation, we suppose that the patterns formed by a stack of three metal patches can response to this need. It is very interesting to examine carefully the resonance configurations with three stacked metallic patches.

References

[1] H. Wang, X. B. Huang, and D. G. Fang, "A microstrip antenna array formed by microstrip line tooth-like-slot-patches," *IEEE Trans. Antennas Propagat.*, vol. 55, pp. 1210-1214, Apr. 2007.

[2] L. Bernard, ''Small-size circularly polarized patch antenna with an opening for a video grenade,'' IEEE

Antennas Wireless Propagat. Lett., vol. 7, pp. 681-684, 2008.
[3] L. Barlatey, J. R. Mosig and T. Sphicopoulos. "Analysis of stacked microstrip patches with a mixed potential integral equation," *IEEE Trans. Antennas Propagat.*, vol. 38, pp. 608-615, May 1990.
[4] K. S. Kona and Y. R. Samii, "Novel probe-feeding architectures for stacked microstrip patch antennas," *Microw. Opt. Technol. Lett.*, vol. 38, no. 6, pp. 467-475, Sept. 2003.
[5] J. T. Bernhard and C. J. Tousignant, ''Resonant frequencies of rectangular microstrip antennas with flush and spaced dielectric superstrates,'' *IEEE Trans. Antennas Propagat.*, vol. 47, pp. 302-308, Feb. 1999.
[6] M. Haridim, D. Shukrun, and H. Matzner, ''A novel broadband triple-layer triangular patch antenna,'' *Microwave Opt. Technol. Lett.*, vol. 40, no. 1, pp. 66-70, Jan. 2004.
[7] T. Fortaki, ''Contribution à l'étude des problèmes de caractérisation des antennes microbandes multicouches sans et avec ouvertures dans les plans de masse,'' Thèse de Doctorat, Université de Constantine, Juin 2004.
[8] T. Fortaki, L. Djouane, F. Chebara, and A. Benghalia, ''On the dual-frequency behavior of stacked microstrip patches,'' *IEEE Antennas Wireless Propagat. Lett.*, vol. 7, pp. 310-313, 2008.
[9] F. Chebbara, M. Amir, and T. Fortaki, ''The effect of a high temperature superconducting patch on a rectangular microstrip antenna,'' *KIEE Journal of Electrical Engineering & Technology*, vol. 4, no. 2, pp. 277-281, 2009.
[10] T.Fortaki, L.Djouane, F.Chebara, and A. Benghalia,: Radiation of rectangular microstrip patch antenna covered with a dielectric layer . International Journal of Electronics september 2008; 95: 989-998.
[11] F. Chebbara, S. Benkouda, and T. Fortaki, ''Fourier transform domain analysis of high T_c superconducting rectangular microstrip patch over ground plane with rectangular aperture,'' *Journal of Infrared, Millimeter, and Terahertz Waves*, vol. 31, pp. 821-832.
[12] K. A. Michalski and D. Zheng, ''Analysis of microstrip resonators of arbitrary shape,'' *IEEE Trans. Microwave Theory Tech.,* vol. 40, pp. 112-119, Jan. 1992.
[13] D. M. Pozar, *Microwave Engineering.* Reading, MA: Addison-Wesley, 1990.
[14] D. M. Pozar, ''Radiation and scattering characteristics of microstrip antennas on normally biased ferrite substrates,'' *IEEE Trans. Antennas Propagat.,* vol. 40, pp. 1084-1092, Sept. 1992.
[15] Q. Liu and W. C. Chew, ''Curve-fitting formulas for fast determination of accurate resonant frequency of circular microstrip patches,'' *Proc. Inst. Elec. Eng.,* vol. 135, no. 5, pp. 289-292, Oct. 1988.
[16] S. A. Long and M. D. Walton, "A dual-frequency stacked circular-disc antenna," *IEEE Trans. Antennas Propagat.*, vol. AP-27, pp. 270-273, Mar. 1979.
[17] U. K. Revankar and A. Kumar, ''Experimental investtigation of three-layer electromagnetically coupled circular mictrostrip antennas,'' *Electron. Lett.,* vol. 27, no. 13, pp. 1187-1189, June. 1991.

F. Chebbara was borne in 1978 in Batna, Algeria. Has Doctoral degree in Electronics from University of Batna, has been a teacher at the University of Ouargla since 2010. His research interstes are: Power electronics, antennas, microbande and transmission.

T. Fortaki was borne in Constantine, Algeria. Has Doctoral degree in Electronics from University of Constantine, has been a teacher at the University of Batna since 2001. He is now Professor. His research interstes are: Study of microwave devices, Study applications of microwave devices, Realization of microwave devices, Power electronics, antennas, microbande and transmission.